Modelling, Analysis, and Design of a Line-Start Permanent Magnet Synchronous Motor

A. Vannini, C. Simonelli, A. Marfoli, L. Papini, P. Bolognesi, C. Gerada

***Abstract*—Line-Start Permanent Magnet Motors are a valid alternative to conventional three-phase induction motors and wound-field synchronous machines for fixed-speed applications direct fed by the grid, targeting superior efficiency and high reliability. A general analytical-numerical approach is presented to model SPM type rotors with embedded squirrel cage, aiming to permit completing both a preliminary design and an effective assessment of the starting and synchronisation capabilities. As a case study, the preliminary design of a 8 MW @ 3000 rpm LSPMSM for large compressors is presented, targeting unity power factor as well as low current THD. The electromagnetic design of the machine is validated by means of a Finite Element (FE) model developed on purpose.**

***Index Terms*—Direct-Start, FE Analysis, Line-Start Synchronous Machines, LSPMSM, PM, Reliability, Squirrel Cage**

I. Introduction

Nowadays, 3-phase Squirrel Cage Induction Motors (SCIMs) are widely used in industrial applications for their robustness and low cost [1]. However, they suffer from relatively low efficiency and power factor. The high performance of permanent magnets (PMs) favored a larger and larger use of PM synchronous motors (PMSMs) in many applications thanks to their high power density and efficiency. However, common PMSMs lack the self-starting capability that is required in conventional applications where the motor is directly fed from the grid, as they need a controlled power converter to get properly supplied. Therefore, the concept of Line-Start Permanent Magnet Synchronous Motor (LSPMSM) was introduced to achieve both the high operational efficiency and compactness of PMSMs and the self-starting capability of SCIMs [2], [3]. Since the motor normally operates at synchronous speed, in such condition the induced currents in the rotor are negligible, meaning that the rotor Joule losses are drastically reduced in comparison to SCIMs. In addition, a proper design permits to achieve unity-power-factor operation at the reference load condition. The Surface mounted Permanent Magnet (SPM) rotor type is preferred for large PMSMs, thanks to its easier manufacturing and robustness [3].

The most accurate tool to assess the self-starting capability of LSPMSM motors is transient with motion Finite-Element Analysis (FEA) due to the induced nature of the currents flowing in the cage during asynchronous operation. However, the accuracy of the FEA comes at the cost of a high computational burden, thus limiting the use of such tool for the design and optimization [4]–[6]. On the other hand, the popular single-phase equivalent circuit of SCIMs [7] or sizing approaches based on lumped parameter magnetic circuits [8], [9] can only be used for the analysis of steady-state conditions or slowly evolving transient. The mid-complexity analytical modelling presented in [10]–[12] allows to describe the behavior of any electro-magneto-mechanical device by means of a lumped-parameters analysis based on state variables. In this paper, such analytical approach is applied to LSPMSMs by combining the numerical implementations previously proposed for SPMs [13] and SCIMs [14]. Then, the preliminary electromagnetic sizing of a LSPMSM is addressed, referring as a case study to a $8\,\mathrm{MW}$ application. The validation carried out by means of Finite-Element Analysis (FEA) is then described, reporting and commenting the results obtained.

Amedeo Vannini, Alessandro Marfoli, and Chris Gerada are with the Power Electronics, Machines, and Control Group, University of Nottingham, UK (e-mail: amedeo.vannini1@nottingham.ac.uk).

Claudia Simonelli, Luca Papini, and Paolo Bolognesi are with the University of Pisa - DESTEC, Italy (e-mail: paolo.bolognesi@ing.unipi.it)

II. Analytical Modelling

A. Background

In [10], [11], the general reference framework of the analytical circuital model approach used to analyse any electro-magneto-mechanical device is presented. Such modelling approach is valid under the following assumptions [12]:

- straight extruded geometry along the machine axis (no skewing) with stator and rotor magnetic cores featuring equal length ℓ much larger than the transversal size;
- negligible MMF drop, hysteresis losses, and eddy currents in the iron cores, permitting to consider the problem as magnetically linear;
- negligible mutual influence between main and secondary field lines, allowing to analyse separately the principal and leakage fluxes;
- SPM layout with roughly radial PM magnetization;
- negligible variation of the magnetic field in the air-gap along the radial direction, permitting to focus on its variation only along the tangential direction;
- cage located close to the rotor surface for maximizing the linkage with the main flux tubes.

According to the previous hypotheses, the voltage equation of the machine can be expressed in matrix form by piling-up the electrical variables related to all of the equivalent phases in the machine [10]:

$$\bar{v}\,(t) = \mathbf{R} \cdot \bar{i}\,(t) + \mathbf{L}(\alpha) \cdot \frac{d\bar{i}\,(t)}{dt} + \bar{M}\,(\alpha, \bar{i}) \cdot \frac{d\alpha\,(t)}{dt} \qquad (1)$$

where t is the time, $\bar{v}$ is the vector of phase voltages, $\mathbf{R}$ is the resistance matrix, $\mathbf{L}$ is the inductance matrix depending only on the Lagrangian variable α describing the rotor vs. stator position, and $\bar{i}$ is the vector of phase currents. The motional coefficient vector $\bar{M}$ is expressed as:

$$\bar{M}\left(\bar{i},\alpha\right)=\frac{\partial\bar{\Psi}\left(\bar{i},\alpha\right)}{\partial\alpha}=\frac{\partial\bar{\Psi}_0\left(\alpha\right)}{\partial\alpha}+\frac{d\mathbf{L}(\alpha)}{d\alpha}\cdot\bar{i} \quad (2)$$

where $\bar{\Psi}$ is the main linkage flux vector function and $\bar{\Psi}_0$ its no-current component [11]:

$$\bar{\Psi}_0(\alpha)=\ell\cdot\int_0^1\mu_e\left(\lambda,\alpha\right)\cdot\bar{N}_e\left(\lambda,\alpha\right)\cdot\bar{\mathscr{F}}_{e0}\left(\lambda,\alpha\right)\,d\lambda \quad (3)$$

In the above equation λ is the variable spanning in the interval $[0,1)$ which is used for the geometrical parametrization of the air-gap average surface along the tangential direction, ℓ is the axial active length and $\bar{\mathscr{F}}_{e0}$ is the equivalent magneto-motive force introduced by the PMs [12]. The equivalent permeability function $\mu_e\left(\lambda,\alpha\right)$, as defined in [12], takes into account the effects of the air-gap size, shape, and anisotropy. The main inductance matrix, related to the main flux tubes crossing the air-gap and linked with the phases, can be then expressed as:

$$\mathbf{L}(\alpha)=\ell\cdot\int_0^1\mu_e\left(\lambda,\alpha\right)\cdot\bar{N}_e\left(\lambda,\alpha\right)\cdot\bar{N}_e^{\mathrm{T}}\left(\lambda,\alpha\right)\,d\lambda \quad (4)$$

where $\bar{N}_e\left(\lambda,\alpha\right)$ is the equivalent winding function given by:

$$\bar{N}_e\left(\lambda,\alpha\right)=\bar{N}\left(\lambda,\alpha\right)-\int_0^1\frac{\mu_e\left(\lambda,\alpha\right)\cdot\bar{N}\left(\lambda,\alpha\right)}{\int_0^1\mu_e\left(\lambda,\alpha\right)\,d\lambda}\,d\lambda \quad (5)$$

The $\bar{N}\left(\lambda,\alpha\right)$ vector function describes the spatial distribution of the active sides of both stator and rotor windings, while the equivalent winding function represents its weighted average value calculated vs. $\mu_e\left(\lambda,\alpha\right)$ [15]. The electromagnetic torque T_E is then determined as the derivative of the electromagnetic coenergy with respect to α, obtaining:

$$T_E\left(\bar{i},\alpha\right)=T_{E0}(\alpha)+\bar{i}^{\mathrm{T}}\cdot\frac{\partial\bar{\Psi}_0\left(\alpha\right)}{\partial\alpha}+\frac{1}{2}\cdot\bar{i}^{\mathrm{T}}\cdot\frac{d\mathbf{L}(\alpha)}{d\alpha}\cdot\bar{i} \quad (6)$$

where T_{E0} is the no-current (cogging) torque.

B. Cage Modelling

As proposed in [14]–[16], the squirrel cage can be modelled as an equivalent planar circuit permitting to apply the analytical approach considered so far, despite the basic hypotheses are apparently not met. For such purpose, the planar representation of a complete cage [15] depicted in Fig. 1 is adopted, where a number of b straight bars is shown in red, whilst the inner and outer connection circles in black represent the two end rings.

According to the graph theory, the currents flowing in the rotor bars and rings can be expressed as functions of the currents associated to the b natural loops, consisting of adjacent bars and their ring connections, and to the loop

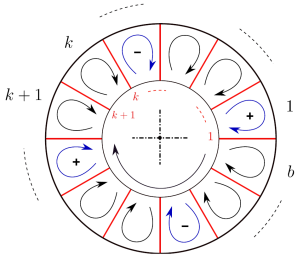

Fig. 1. Planar topology representation for the squirrel cage

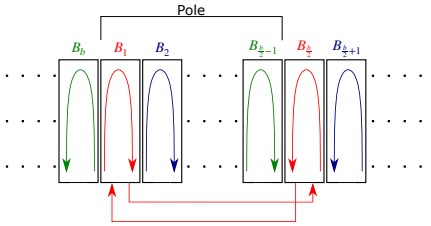

Fig. 2. Simplified representation of the current loops by exploiting the symmetries of the cage in the case of 2 poles structure

corresponding to the inner ring, as depicted in Fig. 1. Each of such natural loops may be considered as an equivalent phase whose terminals are short-circuited: the squirrel cage can be then represented as a set of $b+1$ equivalent phases. When both the stator and the rotor feature a cyclic-symmetrical structure according to the same number of pole pairs p, the currents flowing into cage loops located 2 pole pitches apart can be assumed to be the same in any condition. Moreover, when inside each pole pair an integer number of cage bars is found and the stator structure features an odd cyclic symmetry, then the currents flowing into cage loops that are located 1 pole pitch apart can be assumed to have opposite values at any time. Furthermore, the inner loop current is usually negligible. Therefore, the number of equivalent rotor phases can be drastically reduced from $b+1$ to $b/(2p)$ by connecting in anti-series all of the loops whose currents are related [15], [17], as shown in Fig. 2.

According to the chosen representation, the matrix of the rotor resistances $\mathbf{R}_R$ features a quasi tridiagonal form [14] :

$$\mathbf{R}_R=2p\cdot\begin{bmatrix}R_r & R_m & 0 & \dots & 0 & -R_m\\ R_m & R_r & R_m & 0 & \dots & 0\\ \vdots & \ddots & \ddots & \ddots & \ddots & \vdots\\ 0 & \dots & R_m & R_r & R_m & 0\\ 0 & \dots & 0 & R_m & R_r & R_m\\ -R_m & 0 & \dots & 0 & R_m & R_r\end{bmatrix} \quad (7)$$

where the equivalent values $R_r=2\left(R_b+R_{ring}\right)$ and $R_m=-R_b$ are obtained from the resistances of each bar R_b and of each ring sector delimited by adjacent bars R_{ring}.

On the other hand, the inductance matrix can be evaluated by means of (4), where the equivalent rotor winding functions are modelled according to the representation of cage loops shown in Fig. 2 [17]. As a result of the exploitation of the physical symmetries, the mutual inductances between

equivalent rotor phases result equal to zero, thus further reducing the complexity of the problem [15].

III. Electromagnetic Design for Steady-State

The preliminary electromagnetic sizing of a large LSPMSM is proposed hereafter as a case study referring to a large industrial compressor/pump, according to the specifications listed in Tab. I. In such applications, high reliability and low maintenance under continuous operation are key aspects: therefore, direct grid supply solutions operating at constant speed with direct coupling are often preferred to permit eliminating controlled power converters and gearboxes while reducing the costs, despite no flow regulation capability can be offered by the motor. According to the specifications, the number of pole pairs results equal to $p = 1$.

TABLE I
Case study specifications

Symbol	Parameter	Unit	Value
P_n	Rated Power	MW	8
Ω_n	Rated Speed	rpm	3000
V_n	Rated Grid Voltage	kV	10
f_n	Rated Frequency	Hz	50

Hereafter the electromagnetic sizing focused on synchronous operation is presented; the design of the squirrel cage and related start-up capability is then addressed in Sec. IV.

A. Preliminary Sizing

A simplified sizing algorithm based on [18] was applied: by choosing reasonable values for the power factor and the efficiency, a first target value for the rated current may be obtained. A proper strategy to actually obtain the desired current value under grid supply is then applied by means of the numerical implementation of the analytical model. Since the machine stator core is assumed to be isotropic, the torque target T_E permits to estimate the rotor dimensions (ℓ and r_r) by using the simplified equivalent Lorentz force based approach [18], [19]:

$$T_E = \pi \ell r_r \cdot B_M \cdot A_M \tag{8}$$

when reasonable values are selected for the maximum air-gap flux density B_M and the magnetic loading A_M. The PMs are sized according to the desired maximum air-gap flux density, by neglecting at first the armature reaction. The material selected for the PMs is Sm_2Co_{17} owing to its thermal stability and its high magnetic performances including a large value of coercivity H_C, which is necessary to minimize the potential risk of demagnetization especially during the start-up phase when a large uncontrolled transient is expected.

Given the low number of poles and the necessity to operate directly from the grid, a distributed winding layout using a large number of stator slots is targeted to achieve a more sinusoidal MMF waveform in the air-gap. In fact, this permits to reduce both the currents THD, the torque ripple, and the rotor losses due to undesired eddy currents that could still circulate even at synchronous speed. After suited considerations, the stator winding layout is chosen as a double layer structure deployed in $Q = 36$ evenly spaced slots with coils pitch shortened by $a = 2$ slots. Such solution is chosen as a good trade-off between the maximization of the fundamental component amplitude and the quality of the spectrum of the winding functions. The stator phases are Y connected with isolated center tap, thus permitting to inherently eliminate the current harmonics belonging to the family 3 and to better cope with the rather high supply voltage.

The structure of the rotor is assumed to consist in a cylindrical magnetic core hosting the squirrel cage in suited slots located close to the external profile, surrounded by a layer of permanent magnets. Considering that the differential permeability of the chosen PM material is very close to that of vacuum, from the point of view of steady-state operation the machine can be considered operating as an isotropic PMSM.

B. Design Refinement Through Numerical Resolution

The model presented in the previous section is implemented as a script in the numerical simulation environment Matlab®. The dependency of the functions with respect to the variable λ is numerically implemented as a sampling over 3600 points evenly spaced along the whole air-gap in the tangential direction. Thanks to the low computational burden in comparison to FEA, such model allows to examine many different options in a relatively short time, permitting to refine the preliminary design in an effective way.

To actually obtain the current supply scenario hypothesized for design purposes, the ensuing line-to-line voltages produced by the machine shall match the assumed grid supply at least in terms of fundamental components. Under the hypothesis of standard sinusoidal operative conditions, the well-known expression of the torque in the canonical transformed Park reference frame is:

$$T_E = p \cdot [\Psi_d \cdot i_q + (L_d - L_q) \cdot i_d \cdot i_q] \tag{9}$$

where the *d* and *q* subscripts refer to the components related to the respective axes. Due to the assumed isotropic structure of the machine, one has $L_d = L_q$, meaning that the second term in expression (9) is null. Therefore, the Maximum Torque per Ampere (MTPA) operating condition is obtained when $i_d = 0$. Such operative scenario may be effectively represented in the conventional *d-q* planar diagram sketched in Fig. 3a, where the resistive voltage is neglected.

According to [11], the flux vector $\bar{\Psi}$ may be decomposed into its no-current $\bar{\Psi}_0$ and incremental $\bar{\Psi}_I$ components, with the latter parallel to the current vector $\bar{i}$ since $L_d = L_q$. The corresponding voltage vector $\bar{v}$ features then a quadrature component ($\varphi \neq 0$) determining a power factor which becomes smaller and smaller than 1 as the incremental component of the flux vector becomes prominent with respect to the no-current component due to PMs. Therefore, the MTPA strategy leads inherently to a sub-optimal power factor, which

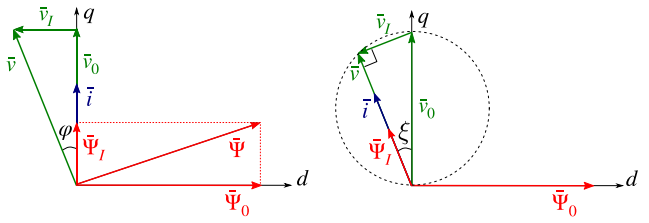

(a) *MTPA strategy* (b) *Adopted strategy:* $\cos\varphi = 1$ *condition*

Fig. 3. Conventional *d-q* planar diagram

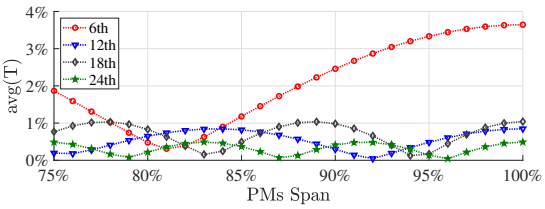

Fig. 4. Amplitude of significant torque ripple harmonics vs. PM span

depends on the operative condition and can approach the value 1 only when the armature reaction results negligible.

On the other hand, in the considered applications the motor is fed by the grid and is expected to operate around its rated condition most of the time. Therefore, it is usually preferable to design the machine in such a way to achieve a power factor close to 1 to mainly benefit the grid, although this departs from the MTPA strategy that permits to maximize the output for any given stator copper losses. When the ideal condition $\varphi = 0$ is achieved, $\bar{\Psi}_I$ is parallel to $\bar{v}$, meaning that one must have $\bar{v} \perp \bar{v}_I$ with an appropriate ratio between the no-current and incremental voltage components. The locus of the possible values of the voltage vector $\bar{v}$ obtained by such condition consists then in the circumference whose diameter is singled out by the vector $\bar{v}_0$, as shown in Fig. 3b.

For a given machine design and current, the appropriate angular deviation ξ of the current vector from the q axis can be calculated keeping in mind that the voltage components $\bar{v}_0$ and $\bar{v}_I$ are proportional to the corresponding amplitudes of flux density components B_{GI} and B_{G0}, respectively. Therefore, from the geometrical relations reported in Fig. 3b, one obtains:

$$\xi = \arcsin\left(\frac{B_{GI}}{B_{G0}}\right), \qquad i_d = -|\bar{i}| \cdot \cos\xi \tag{10}$$

In such conditions, the amplitude of the fundamental component of the total voltage is [1] $v = |\bar{v}_0| \cos\xi$, thus resulting smaller than the no-current voltage. Since the fluxes are proportional to the machine active length ℓ, such parameter acts as a scaling factor for the voltages without altering the power factor: therefore, such dimension can be adjusted during the design process to match the rated voltage of the machine. Anyway, any adjustment of ℓ affects also the torque provided by the machine: this was also taken into account.

The angular span of the PMs was selected after numerically analysing its impact on the torque ripple at rated conditions by using (6), under the assumption of sinusoidal 3-phase symmetrical current supply. The most significant low-order harmonics of the ripple spectrum were calculated vs. the PM span, as shown in Fig. 4: such parameter was then selected as $\tau_{PM} = 82\%$ of the pole pitch. The attenuation of harmonic 36 due to slotting was addressed separately.

The main results obtained from the preliminary design procedure are reported in Tab. II.

TABLE II
PRELIMINARY SIZING OUTPUTS

Symbol	Parameter	Unit	Value
ε_G	Air-gap Thickness	mm	8
ε_M	PMs Thickness	mm	27
τ_{PM}	PMs Span	-	82%
ℓ	Active Axial Length	mm	1690
D_r	Rotor External Diameter	mm	757
D_s	Stator External Diameter	mm	1367
N_s	Number of Stator Turns	-	24
Q	Number of Slots	-	36
a	Pitch Shortening	-	2
w_t	Tooth Width	mm	43
k_{fill}	Slots Fill Factor	-	0.4
J_s	Max. Stator Current Density	$\mathrm{A/mm^2}$	4

C. Design validation via FEA

The results provided by the analytical-numerical model described in the previous section were validated by means of a 2D electromagnetic model purposely developed within the specialized software JMAG®. In Fig. 5, the FE model of the designed machine is shown with the related solution mesh. The assumption of anti-symmetrical machine structure was exploited to minimize the computational burden by modeling just half of the tangential span and imposing odd angular periodic boundary conditions along the cut line. The first validation involved the steady-state operation: therefore, at this stage the rotor bars conductivity was set to zero.

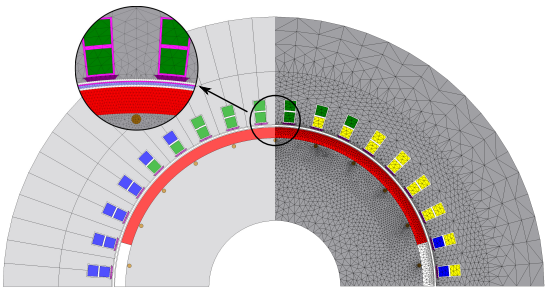

Fig. 5. 2D-FE model with a mesh representation

The validation of stator inductances calculations was carried out first, obtaining very good results. As example, the trend of a stator phase self-inductance with respect to the rotor position is reported in Fig. 6: an excellent match can be observed, with a very small fluctuation as expected in case of isotropic machines.

A further validation was carried out concerning the no-current voltages generated at rated speed. For such purpose

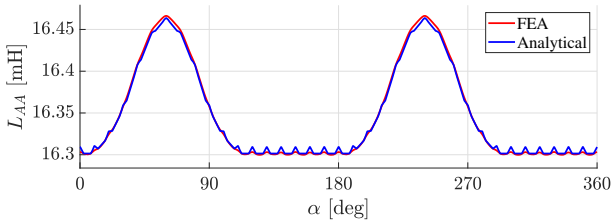

Fig. 6. Stator self-inductance validation: analytical model vs. FE

speed-driven transient-with-motion simulations were carried out: the results obtained highlighted a pretty good general match, although the effect of slot opening turned out to be over-estimated by the analytical-numerical calculations, as reported in Fig. 7.

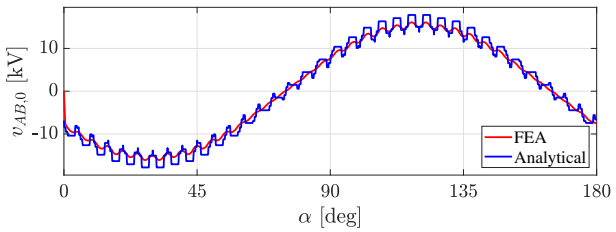

Fig. 7. Line-to-line back-EMF across phase A and B

Both discrepancies can be at least partly attributed to not so negligible MMF drops within the iron cores especially in the parts closer to saturation. Anyway, the FEA confirmed the effectiveness of the double-layer winding configuration with relatively large number of slots adopted, which permits to achieve an actual voltage waveform that is pretty smooth and rather close to the targeted sinusoidal trend.

The sizing of magnetic parts was then assessed at steady state by running transient-with-motion simulations at the rated speed imposing symmetrical sinusoidal stator currents according to the desired operative scenario discussed in Section III-B. The field map obtained is reported in Fig. 8: the flux density matches pretty well with the expectations.

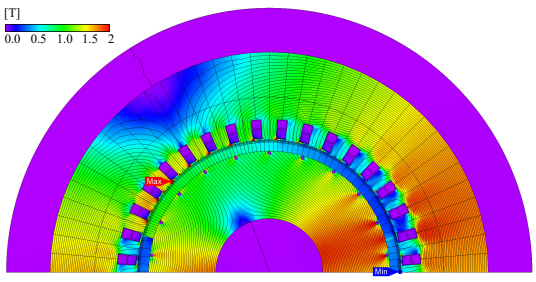

Fig. 8. Field map at the synchronous operative point

D. Magnetic wedges

As a possible improvement, the adoption of semi-magnetic slot wedges ($\mu_r = 10$ [20]) was investigated to further reduce the voltage and torque ripple. In Fig. 9 the torque trends obtained by FEA with and without semi-magnetic wedges are compared to the average value predicted by the analytical model: the wedges permit both to slightly increase the average value and to significantly reduce the torque ripple due to slotting, i.e. the harmonic family 36.

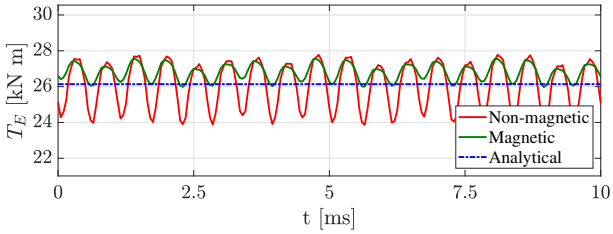

Fig. 9. FEA torque ripple vs. wedges material and analytical average value

IV. Design for Start-Up

The analytical model proposed in Sec. II can be implemented in the Matlab-Simulink® environment in order to predict the dynamic start-up performance considering various operative conditions and rotor cage structures, targeting the self-start requirements of the application under study. At this stage, an ideal grid scenario is considered. Then, the design of the cage is refined and finalised through FEA, aiming to fulfil the requirement of safe and robust starting capability.

A. Numerical-Analytical Implementation

The block diagrams of the electromagnetic and electromechanical parts of the Matlab-Simulink® dynamic model implemented for analyzing the dynamic behavior of the machine are shown in Fig. 10a and 10b, respectively.

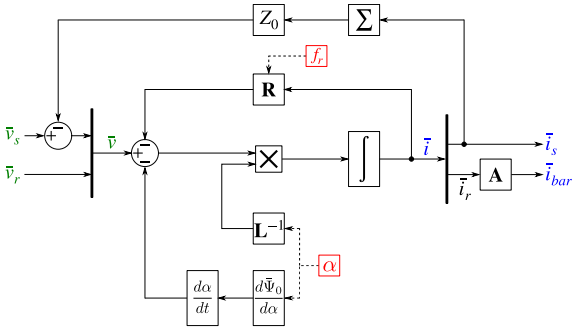

(a) *Electromagnetic dynamic*

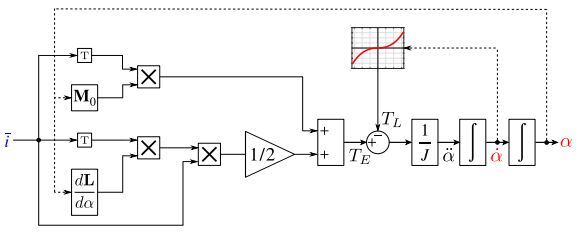

(b) *Electromechanical dynamic*

Fig. 10. Schematic block-diagram representation of the dynamic model numerically implemented in the Matlab-Simulink® environment

The voltage vector $\bar{v}$ is split into the stator and rotor components, namely $\bar{v}_s$ and $\bar{v}_r$, respectively. The former is imposed by the grid, assumed as a 3-phase ideal voltage supply system, while the latter is null due to the short-circuited structure of the cage. The feedback loop at the top emulates the effect of the isolated center tap for the Y connected stator phases by means of a suited large impedance Z_0 [17]. The inverse of the matrix of inductances $\mathbf{L}^{-1}$, as well as the derivative of the no-current fluxes vector, were pre-calculated and then stored as position-dependent look-up tables.

The selection of an optimal shape for the cross-section of the rotor bars is a significant design aspect [1], but it goes beyond the objective of this paper. However, a round cross-section is considered a reasonable choice for the sake of simplicity, and in double-cage SCIMs it is often employed for the external one dedicated to improve the start-up capability of the machine. The rotor bars equivalent resistances are dependent on rotor frequency f_r, and their value is estimated as proposed in [21] for round bars. The $\mathbf{A}$ matrix relates the loop currents $\bar{i}_r$ with the bar currents $\bar{i}_{bar}$.

The selection of the number of bars b, as well as their their diameter D_b and material, significantly affects the starting capability of the machine [18]. Such design variables were investigated by comparing several different combinations, thanks to the low computational burden required by the above model. Since the purpose of the cage is just limited to start-up, choosing a relatively high-resistivity material appears interesting for both boosting the torque, reducing the transient currents and reducing the losses at synchronous operation: the popular brass alloy including 58% Cu ($\rho = 5.9 \times 10^{-8}\,\Omega \cdot \mathrm{m}$) was then selected as a cost effective solution.

In Fig. 11, the speed trend during the start-up transient is reported for some significant cases, assuming a mechanical load featuring a quadratic torque vs. speed characteristic, typical of large industrial compressors. It can be noticed that a rotor cage featuring higher bar resistance (i.e. smaller diameter) determines a higher starting torque, thus decreasing the start-up time; on the other hand larger values of D_b may help reducing both the overshoot and the oscillations amplitude. As example, a failed startup is also shown in orange. The combination $\{b = 22;\ D_b = 14\,\mathrm{mm}\}$ providing the trend in magenta was finally singled out as a promising compromise, since it determines a fast synchronisation with good damping.

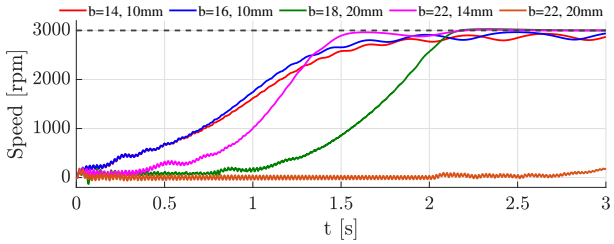

Fig. 11. Starting simulations for different cage designs: speed vs. time. The number of bars as well as their diameter is reported

B. Model validation via FEA

The proposed analytical modeling relies on the assumed hypotheses. However, such assumptions could prove to be inaccurate especially during the first instants of the starting transients, when complex and interacting phenomena emerge. More accurate results can be provided by FEA voltage-fed transient-with-motion simulations, permitting also to assess any kind of risk of demagnetization of the PMs during the starting transient. They were carried out using the 2D model previously described, modeling the bars as solid conductors connected in parallel and considering both linear and saturable magnetic materials for the cores. A comparison of the speed trends provided by FEA and analytical model during the startup for the selected cage sizing is reported in Fig. 12.

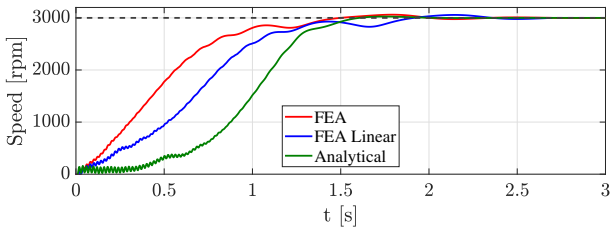

Fig. 12. Ideal grid start-up speed transient: FE vs. analytical

Significant time displacements emerge among the 3 speed ramps, meaning that the cage operation is not fully caught and that saturation also plays a not negligible role; nevertheless, the slope of the ramps looks very similar. Moreover, the predicted operation at $\cos\varphi = 1$ is confirmed by FEA with good accuracy, as one can notice in Fig.13 comparing the phase voltage and current trends achieved at steady state. Furthermore, the design proved to be quite fine also from the point of view of the current waveform quality, since it looks almost sinusoidal with a very low value of $\mathrm{THD}_I = 0.33\%$.

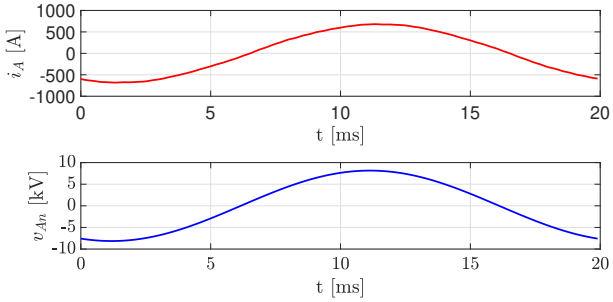

Fig. 13. Steady-state phase current (in red) and voltage (in blue) waveforms evaluated from start-up simulation within FE environment , related to the phase labelled as A

Finally, it is worth comparing the computational time required for running the two models on the same PC: the numerical-analytical model takes a far smaller time (about 12s vs. 6.5h for linear FEA and 9h for non-linear FEA), despite providing a much larger number of time samples (300 000 vs. 4120), thus confirming its usefulness as an attractive balance between accuracy and speed.

V. Conclusions

In this paper an analytical-numerical model permitting to analyze and design LSPMSMs featuring a SPM rotor layout with round cross-section bars was presented. As a case study, it was applied to the preliminary electromagnetic design of a 8 MW LSPMSM focusing on the power quality aspect, i.e. low current THD and unity-power factor. The results obtained were validated against FEA using a 2D model developed on purpose, proving that the proposed method permits to describe rather accurately the synchronous operation with a reduced computation time. Future work will be focused on the improvement of the transient results, which anyway are still useful to discriminate unsuited solutions at preliminary design stage.

Acknowledgements

The authors would like to appreciate the support of JSOL Corporation for providing Jmag-Designer as motor design software.

References

[1] A. Marfoli, M. D. Nardo, M. Degano, C. Gerada, and W. Jara, "Squirrel cage induction motor: A design-based comparison between aluminium and copper cages," *IEEE Open Journal of Industry Applications*, vol. 2, pp. 110–120, 2021.

[2] W. Fei, P. C. K. Luk, J. Ma, J. X. Shen, and G. Yang, "A high-performance line-start permanent magnet synchronous motor amended from a small industrial three-phase induction motor," *IEEE Transactions on Magnetics*, vol. 45, no. 10, pp. 4724–4727, 2009.

[3] P. W. Huang, S. H. Mao, M. C. Tsai, and C. T. Liu, "Investigation of line start permanent magnet synchronous motors with interior-magnet rotors and surface-magnet rotors," in *2008 International Conference on Electrical Machines and Systems*, 2008, pp. 2888–2893.

[4] A. J. Sorgdrager, R.-J. Wang, and A. J. Grobler, "Multiobjective design of a line-start pm motor using the taguchi method," *IEEE Transactions on Industry Applications*, vol. 54, no. 5, pp. 4167–4176, 2018.

[5] D. Mingardi and N. Bianchi, "Line-start pm-assisted synchronous motor design, optimization, and tests," *IEEE Transactions on Industrial Electronics*, vol. 64, no. 12, pp. 9739–9747, 2017.

[6] B. Zöhra, M. Akar, and M. Eker, "Design of a novel line start synchronous motor rotor," *Electronics*, vol. 8, no. 1, 2019. [Online]. Available: https://www.mdpi.com/2079-9292/8/1/25

[7] D. Genovese, P. Bolognesi, M. De Martin, and F. Luise, "A contextual parameter identification method for the equivalent circuit of induction machine," in *2016 XXII International Conference on Electrical Machines (ICEM)*, 2016, pp. 25–31.

[8] A. Waheed and J.-S. Ro, "Analytical modeling for optimal rotor shape to design highly efficient line-start permanent magnet synchronous motor," *IEEE Access*, vol. 8, pp. 145 672–145 686, 2020.

[9] X. Lu, K. L. V. Iyer, K. Mukherjee, and N. C. Kar, "Development of a novel magnetic circuit model for design of premium efficiency three-phase line start permanent magnet machines with improved starting performance," *IEEE Transactions on Magnetics*, vol. 49, no. 7, pp. 3965–3968, 2013.

[10] P. Bolognesi, "Generalized circuital modeling of electromechanical devices," in *Proc. ICEM 2004 Conf*, 2004.

[11] P. Bolognesi, "Generalized analysis of electromechanical devices using pseudo-linear transformations," in *Proc. ICEM 2006 Conf*, 2006.

[12] P. Bolognesi, "A mid-complexity analysis of long-drum-type electric machines suitable for circuital modeling," in *2008 18th International Conference on Electrical Machines*, 2008, pp. 1–5.

[13] F. Papini and P. Bolognesi, "Preliminary design and analysis of a high speed permanent magnets synchronous generator," in *Melecon 2010 - 2010 15th IEEE Mediterranean Electrotechnical Conference*, 2010, pp. 1198–1203.

[14] A. Marfoli, L. Papini, P. Bolognesi, D. Genovese, and C. Gerada, "Analysis of induction machine: Comparison of modelling techniques," in *2017 IEEE International Electric Machines and Drives Conference (IEMDC)*, 2017, pp. 1–7.

[15] S. Nuzzo, P. Bolognesi, M. Galea, and C. Gerada, "A hybrid analytical-numerical approach for the analysis of salient-pole synchronous generators with a symmetrical damper cage," in *2017 IEEE International Electric Machines and Drives Conference (IEMDC)*, 2017, pp. 1–8.

[16] A. Munoz and T. Lipo, "Complex vector model of the squirrel-cage induction machine including instantaneous rotor bar currents," *IEEE Transactions on Industry Applications*, vol. 35, no. 6, pp. 1332–1340, 1999.

[17] A. Marfoli, L. Papini, P. Bolognesi, and C. Gerada, "An analytical-numerical approach to model and analyse squirrel cage induction motors," *IEEE Transactions on Energy Conversion*, vol. 36, no. 1, pp. 421–430, 2021.

[18] V. H. J. Pyrhonen, T. Jokinen, *Design of Rotating Electrical Machines*. John Wiley and Sons, Ltd, 2013.

[19] G. Devito, S. Nuzzo, D. Barater, G. Franceschini, L. Papini, and P. Bolognesi, "Design of the propulsion system for a formula sae racing car based on a brushless motor," in *2021 IEEE Workshop on Electrical Machines Design, Control and Diagnosis (WEMDCD)*, 2021, pp. 318–324.

[20] M. Dems, K. Komeza, and J. Sykulski, "Analysis of effects of magnetic slot wedges on characteristics of large induction motor," *Przeglad Elektrotechniczny*, vol. 88, pp. 73–77, 07 2012.

[21] M. M. Al-Asadi, A. P. Duffy, A. J. Willis, K. Hodge, and T. M. Benson, "A simple formula for calculating the frequency-dependent resistance of a round wire," vol. 19, no. 2, 1998, pp. 84–87.

Biographies

Amedeo Vannini received the M.Sc. (*cum laude*) in Electrical Engineering from the University of Pisa, Italy, in 2020. He enrolled then in the Ph.D. in Electrical Engineering at the University of Nottingham, UK. His main research interests include the modelling, analysis and design of electric machines, in particular permanent magnet, induction and homopolar, for various applications including industrial motors and generation systems.

Claudia Simonelli received the M.Sc. (*cum laude*) in Electrical Engineering from the University of Pisa (Italy) in 2019, where she is currently pursuing the Ph.D. in Electrical Engineering and Applied Electromagnetism. Her research interests mainly involve the analysis and modelling of magnetorheological fluids and spherical induction motors haptic devices.

Alessandro Marfoli received the M.Sc. in Electrical Engineering from the University of Pisa, Italy, in 2015, and the Ph.D. degree in electrical machine design from the University of Nottingham (UK) in 2020 where he is currently a Research Fellow. His main research interests include modelling, analysis and optimization of electrical machines.

Luca Papini received the bachelor's (Hons.) and master's (Hons.) degrees in Electrical Engineering from the University of Pisa, Italy, in 2009 and 2011, respectively, and the Ph.D. degree from the University of Nottingham, U.K., in 2018. He has been a Research Assistant with the University of Nottingham, since 2013. He was JSPS Fellow in 2018 and is currently a Senior Researcher with the University of Pisa. His research interests include high-speed, high power density electric machines, machine control, and levitating systems.

Paolo Bolognesi received the M.Sc. in Electrical Engineering *cum laude* and the Ph.D. degree from the University of Pisa, Italy, in 1995 and 1999 respectively. Since 2001 he is with the University of Pisa as a Senior Researcher and Appointed Professor. His research interests are mainly focused on the theoretical and simulation modeling and analysis of electro-magneto-mechanical devices and on their design. He is also interested in innovative topologies and modulation/control techniques for power converters and drives, as well as in specific applications such as electric and hybrid vehicles, aerospace, industrial automation and renewable energies.

Chris Gerada received the Ph.D. degree in numerical modelling of electrical machines from the University of Nottingham, U.K., in 2005. He subsequently worked as a Researcher with the University of Nottingham on high-performance electrical drives and on the design and modelling of electromagnetic actuators for aerospace applications. He was appointed a Lecturer in electrical machines in 2008, an Associate Professor in 2011, and Professor in 2013. His core research interests include the design and modelling of high-performance electric drives and machines. Prof. Gerada is an Associate Editor of the IEEE Transaction on Industry Applications. He has secured major industrial, European and U.K. grants, authored more than 200 papers and was awarded a Royal Academy of Engineering Research Chair to consolidate research in the field.